

SANS Analysis of the Microstructural Evolution during the Aging of Pyrolysis Oils from Biomass

Emiliano Fratini^a, Massimo Bonini^a, Anja Oasmaa^b, Yrjo Solantausta^b and Piero Baglioni^{a,}*

- a. Department of Chemistry and CSGI, University of Florence, Via della Lastruccia 3, I-50019 Sesto Fiorentino, Firenze, Italy
- b. VTT Processes, P.O. Box 1601, 02044 VTT, Finland

*Corresponding author. Phone: +39-055-457-3033 Fax: +39-055-457-3032.

E-mail: piero.baglioni@unifi.it. Internet: <http://www.csgi.unifi.it>

ABSTRACT (Word Style “BD_Abstract”). All manuscripts must be accompanied by an abstract. The abstract should briefly state the problem or purpose of the research, indicate the theoretical or experimental plan used, summarize the principal findings, and point out major conclusions. The optimal length is one paragraph.

KEYWORDS (Word Style “BG_Keywords”). If you are submitting your paper to a journal that requires keywords, provide significant keywords to aid the reader in literature retrieval.

Introduction

The energetic scenario depicted by most analysts urges researchers for establishing new technologies based on renewable energy (RE) sources in the next few years. Among the possible RE sources, Bio Crude Oils (BCOs) have attracted a considerable attention. These oils are obtained by the pyrolysis of biomass: i.e. heating of the feedstock (this includes various materials, such as wood and agricultural wastes, paper, algae, animal wastes, etc.), followed by a rapid quenching of the liquid products^{1,2}.

At the moment, one of the most interesting applications of pyrolysis of biomass consists in the flash pyrolysis of wood, both as saw dust or forestry residues. Oils obtained by this technique are good candidates as potential substitutes for fossil fuels: in particular they have already been used in modified diesel engines³. Unfortunately, direct utilization of BCOs in internal combustion systems requires significant adaptations in both their design and components: in fact, the low pH value of these oils makes them strongly aggressive to the metallic parts, unless built in stainless steel. Various processes have been recently proposed in order to upgrade these alternative fuels^{4,6}. Among these, the emulsification of BCOs with Diesel oil represents an interesting option^{7,8}: this approach allows the use of low-cost diesel engines with only minor modifications, thus reducing significantly the investment costs⁹.

In view of their use as substitutes for fossil fuels (both as pure oils or as part of a stable emulsion), the major problem affecting BCOs is represented by their poor storage stability: in fact, the numerous reactions taking place after the production make them very reactive and cause many problems in their handling and utilization. In particular, compared to conventional petroleum-derived fuels, pyrolysis oils show a lower long-term stability and a relevant dependency on the storage temperature¹⁰. Therefore the characterization of the composition of BCOs and the way it is affected by aging represents a crucial step in order to allow the usability of these oils in technical applications.

In general, these oils are formed by a large number of organic compounds, mainly carboxylic acids, carbohydrates and lignin derived substances, together with a variable amount of water. Unfortunately some of these organic compounds are very reactive and seem to be the major responsible for the ageing process¹¹: in fact during storage these reactive components can interact to form larger molecules and consequently cause changes in crucial physical properties such as viscosity and density.

In previous studies it was proposed that the chemical reactions taking place in the pyrolysis oils are mainly etherifications and esterifications occurring between hydroxyl, carbonyl, and carboxyl groups¹², with water formed as a byproduct of the condensation reactions.

Lignin derived compounds are indicated as *pyrolytic* lignins and they are obtained as the water-insoluble fraction of BCO¹³. It has been shown¹⁴ that the basic units of pyrolytic lignins have significant similarities with milled wood lignins (MWL), making so possible to use the large knowledge about MWL to the characterization of pyrolytic lignins.

Lignin is a heterogeneous polymer, containing minor amounts of extractives and inorganic materials and it is mainly constituted by three basic units: *p*-cumaralcohol, coniferylalcohol and sinapilalcohol (see figure 1). These compounds differ only in the degree of methylation and, since their polymerization gives rise respectively to *p*-hydroxyphenyl lignin (H), guaiacyl lignin (G) and syringil lignin (S), they are also indicated as H, G and S units.

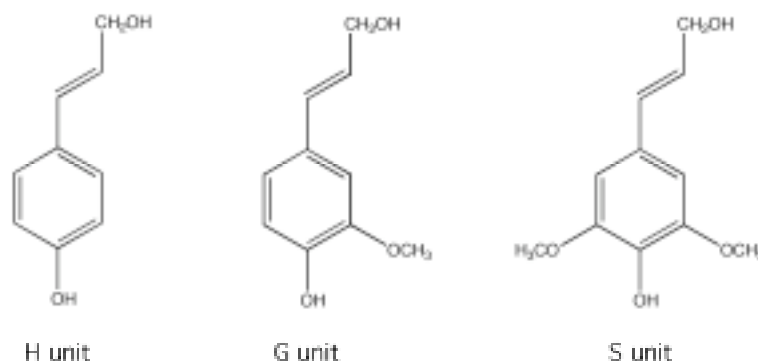


Figure 1. Main constituents of lignines.

It has been previously shown by means of GPC and ¹³C-NMR measurements¹⁵ that pyrolytic lignins consist mainly of trimers and tetramers and that some structural units remain intact during the pyrolysis. These results are consistent with the thermal ejection theory¹⁶, where lignin oligomers are directly ejected from wood particles as a result of a partial cracking of lignin molecules during the pyrolysis.

Aim of this work is to verify the validity of this theory and to elucidate the role of pyrolytic lignines in the ageing of BCO. In particular, the possibility to correlate the aggregation between pyrolytic lignines with the evolution of the BCO's chemico-physical properties would be of outstanding importance: in fact, the demonstration that the aggregates responsible for the ageing of BCOs are constituted by pyrolytic lignines and a deeper knowledge of their mutual interactions would represent a fundamental step ahead in the formulation of pyrolysis fuels characterized by a long-term stability.

In this paper we report for the first time the characterization of a pyrolysis oil by means of small angle scattering of neutrons (SANS). In more details, the oil under investigation was obtained from the pyrolysis of a pine sawdust feedstock. Small angle scattering techniques have been widely used in the last decades as a fundamental tool to characterize mesoscopic structures in solution. In particular SANS was used to study a problem somehow similar to polymerization of pyrolytic lignines: i.e. deposition during heavy oil production^{17,18}. The formation of these deposits depends on the self-association of the heavy components of the crude oil. Among these, asphaltenes have attracted a considerable attention because of their strong propensity to form insoluble aggregates. In a previous study, Chen and coworkers¹⁷ successfully developed a fractal model in order to simulate SANS results of dispersions of asphaltene in toluene at various volume fractions. In another paper¹⁸, the possibility to analyze the results of SANS measurements on asphaltene solutions in toluene at various temperatures according to polydisperse spherical and cylindrical models was successfully explored.

In this study we report the analysis of SANS results using both the fractal and the cylindrical-ellipsoidal models. In both cases the results of the fitting are discussed in terms of goodness of the fit and in terms of the chemico-physical meaning of the results. The hypothesis of the thermal ejection of oligomers of lignines and their aggregation is finally correlated to SANS results.

Materials and Methods

The BCO investigated in this work was produced by VTT (Espoo, Finland), the feedstock being pine sawdust. After the production, BCO was aged at room temperature. A small amount of the fresh BCO was immediately frozen. The same procedure was repeated after 3, 6 and 18 months. Then all the four samples were unfrozen and aged again for 1 month at room temperature before the measurements were performed.

Yrio and Anja: here is where you should put all the details and references regarding the preparation of the oil we have studied and your PDU. Since we want to send this paper to a journal that is not really specific on POs, but it's a little bit more oriented on general chemistry of materials, we think that would be worthy to add a little bit more about your unit and the feedstock than you normally do when you send paper to *Energy and Fuels*-like journals.

Small angle neutron scattering (SANS) measurements were performed on the PAXE spectrometer of the Laboratoire Léon Brillouin at Saclay (France) using two different configurations. The high Q configuration had an average wavelength of 4.5 Å with a sample to detector distance of 1.55 m. The low Q configuration, partially overlapping the previous one, consisted in an average wavelength of 8 Å with a sample to detector distance of 5.05 m. The wavelength spread, $\Delta\lambda/\lambda$, was in both cases less than 10%. The overall Q range investigated for all samples was $0.0075 < Q < 0.33 \text{ \AA}^{-1}$. Scattered neutrons were detected by a two-dimensional XY position detector with 64 x 64 active elements (BF₃) covering a total area of 4096 cm². The beam size at the sample position was circular with a diameter of 7 mm. The intensity, corrected for the empty cell contribution, transmission, and detector efficiency, was normalized to absolute scale by a direct measurement of the intensity of the incident neutron beam. The integration of the normalized 2-D intensity distributions with respect to the azimuthal angle yielded the 1-D scattering intensity distributions, $I(Q)$, in the units of a differential cross section per unit volume of the sample (cm⁻¹). Samples were contained in 1mm circular quartz cells (Hellma) at room temperature (25 °C). The data reduction has been performed using standard routines available at LLB.

Results and Discussion

In figure 2 all the SANS spectra are shown together. It's interesting to notice that the scattered intensity increases with ageing time during the first seven months, while the 7 and 19 months old spectra are almost overlapped.

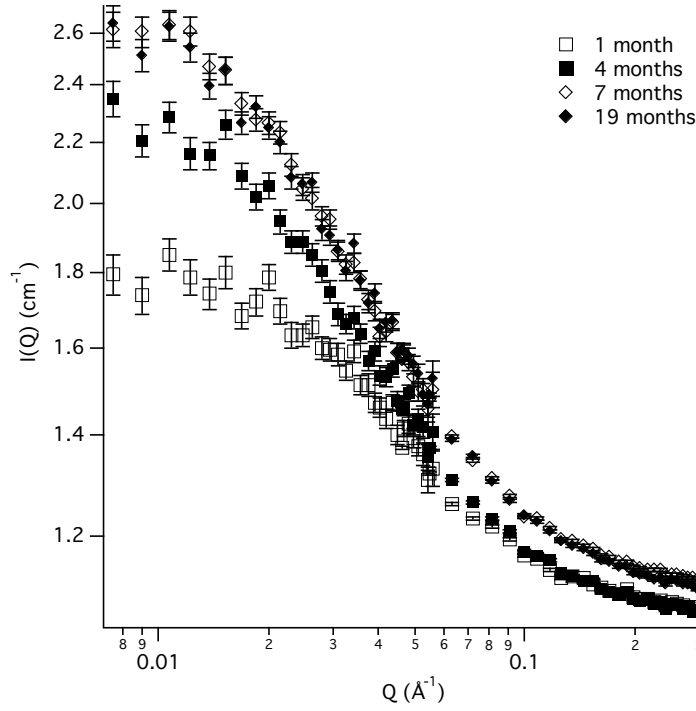


Figure 2. SANS spectra of 1, 4, 7 and 19 months aged samples.

This behavior is consistent with an increase in the number and/or the dimension of the scattering objects and it can be highlighted by looking at the Guinier plots of the spectra (see figure 3): i.e. the natural logarithm of the scattered intensity plotted versus the square of the scattering vector Q^{219} . In these plots the presence of a linear trend in the low Q region can be used to obtain directly the radius of gyration: in fact, in the region of the spectrum where the condition $Q_{\max} \cdot R_G < 1$ is satisfied, the radius of gyration of the scattering object can be obtained directly from the slope of this trend line from the equation:

$$I(Q) = I(0)e^{-\frac{R_G^2 Q^2}{3}} \quad (1)$$

The results of the best fits according to equation 1 are reported in the figure 3. The radius of gyration for the 1 month old sample is $21.0 \pm 1.5 \text{ \AA}$, it goes up to $31.5 \pm 0.9 \text{ \AA}$ for the 4 months old sample and it is almost identical for the 7 and 18 months old samples ($34.5 \pm 0.8 \text{ \AA}$ and $34.1 \pm 0.8 \text{ \AA}$, respectively). It is worthwhile to remind that the Guinier analysis by itself gives no information about the shape of the scattering objects. Moreover, since we do not know *a priori* what are the dimensions of the objects suspended in the BCO, we do not know if the $Q_{\max} \cdot R_G < 1$ condition is effectively satisfied: i.e. we can't be sure that the Guinier analysis provide us with a *real* radius of gyration. In any case, owing to the

presence of a linear trend in the lowest Q region, we can safely calculate a so-called *apparent* radius of gyration. Therefore we can conclude that the dimensions of the scattering objects suspended in the BCO under investigation increase during the first seven months, while no ulterior growth is detectable during the next year. This conclusion doesn't necessarily mean that these objects can aggregate and form structure as big as about 35 Å in radius and then their dimensions do not increase any more: in fact another interpretation of these results would be that structures bigger than a certain dimension are not stable in BCO any longer and they precipitate. This interpretation is supported by the visual inspection of the investigated samples, where the formation of a small precipitate in the oldest sample was detected. In any case, the magnitude of the precipitation phenomenon is almost negligible: in fact, 19 months old sample do not show the decrease in the scattered intensity that should be expected in case of a diminished amount of scattering objects.

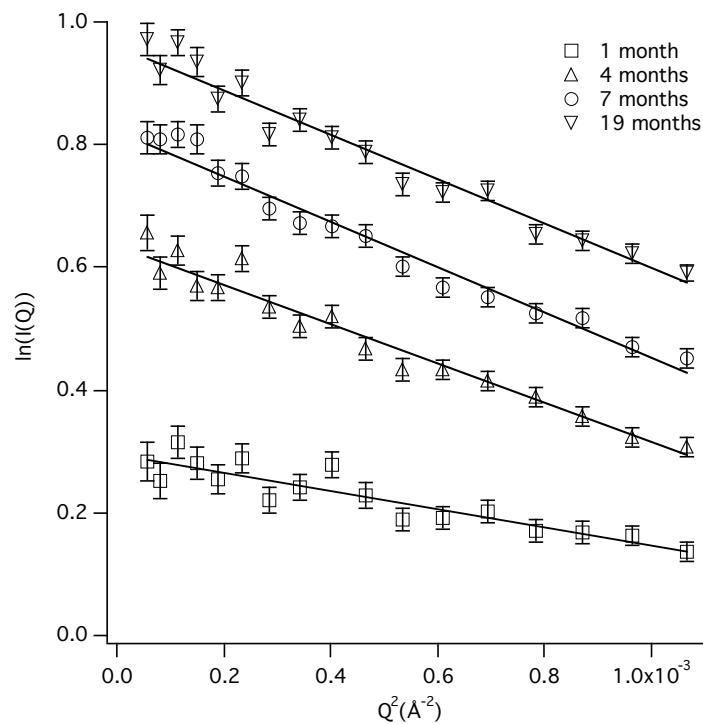


Figure 3. Guinier plots of the low Q region of the SANS spectra of 1, 4, 7 and 19 months aged samples. An offset equal to -0.3 , -0.2 and -0.15 was applied to 1, 4, and 7 months old samples, respectively.

As already mentioned in the introduction, experimental data were fitted according to different models: cylindrical particles, ellipsoidal particles and fractal aggregates of spherical particles. All the details of these

models are reported in the appendix A, while appendix B describes how the contrast (see appendix A) has been calculated.

As a first approach, we tried to fit SANS data accordingly to polydisperse spheres¹⁸. Unfortunately this model showed to be not able to simulate our SANS data (results are available as supporting material).

The results of the fitting obtained by using the cylindrical model are reported in figure 4. For clarity of presentation, both experimental data and fittings of 4, 7 and 19 months old samples are conveniently offset.

Most significant parameters resulting from the fitting routine are reported in table 1.

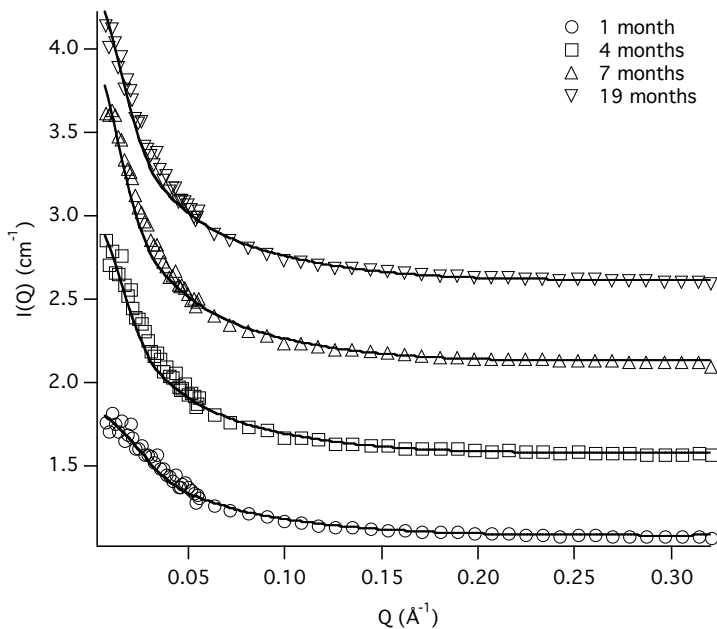


Figure 4. Fitting curves according to the cylindrical model (full lines) and experimental data (markers) of 1, 4, 7 and 19 months aged samples of BCO. 4, 7 and 19 months old sample data and fittings are offset respectively by a 0.5, 1 and 1.5 value.

In all four cases cylinders with a radius of about 14 Å results from the routine, while the volume fraction of scattering bodies increases with ageing time (see table 1). Interestingly there is a clear growth in the length of these cylinders during the first seven months (especially during the first 4 months) but not in their radius, while there is a slight decrease during the successive year. It is important to note that the value of χ^2/n increases continuously with the aging time: i.e. the cylinder model becomes less able to simulate experimental data as the sample ages.

Table 1. Results obtained by fitting SANS experimental data according to a cylindrical model (see Appendix A). In the last line the value of χ^2 divided by the number of experimental points is reported.

Cylinder Model Results				
<i>Ageing Months</i>	1	4	7	19
<i>Volume Fraction</i>	0.088	0.093	0.102	0.113
<i>Radius</i>	13.1	14.3	14.6	13.9
<i>Length</i>	147.6	221.6	245.3	227.2
χ^2/n	4.5	8.8	9.6	11.26

In figure 5 the curves obtained by fitting the experimental data according to an ellipsoidal model are shown. In this case, ellipsoidal structures with minor axes values close to 15 Å and major axes ranging from about 100 and 150 Å were found.

Comparing these results with the cylinder model results, it's very interesting to note how close the volume fraction results are (see table 2). Again the value of χ^2/n increases as a function of ageing time, indicating that also the ellipsoidal model simulates better the fresh samples than the old ones.

Another similarity with the cylinder results is the apparent mono-dimensional growth of the aggregates: i.e. the major axis value increases with ageing, while the minor axis variation is really moderate. The values of χ^2/n are quite similar too, but in the case of the ellipsoidal model are lower than in the cylinder case. We can therefore conclude that both models give good results in describing the concentration and the shape of the objects dispersed in the PO, especially in the case of the first months after the production. Moreover, both cylinders and ellipsoids do not exactly describe the shape of the particles and, in particular, their growth during the ageing.

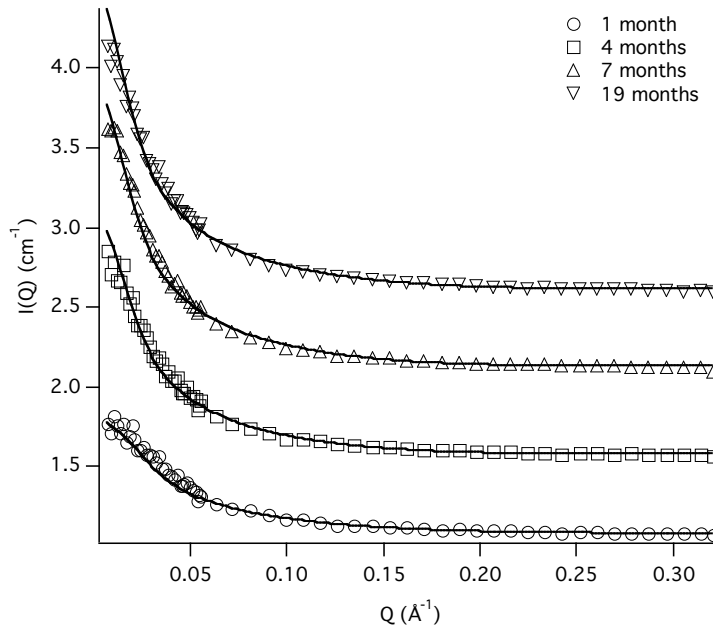


Figure 5. Fitting curves according to the ellipsoidal model (full lines) and experimental data (markers) of 1, 4, 7 and 19 months aged samples of BCO. 4, 7 and 19 months old sample data and fittings are offset by a 0.5, 1 and 1.5 value, respectively.

Table 2. Results obtained by fitting SANS experimental data according to an ellipsoidal model (see Appendix A).

Ellipsoid Model Results				
<i>Ageing Months</i>	1	4	7	19
<i>Volume Fraction</i>	0.091	0.098	0.108	0.121
<i>Major Axis</i>	97.6	143.4	150.0	153.4
<i>Minor Axis</i>	13.5	15.5	15.4	14.7
χ^2/n	3.6	7.2	7.2	9.18

As pointed out in the introduction, experimental data were fitted according to the fractal model developed by Chen and coworkers¹⁷. All the mathematical details of the model are reported in appendix A. In any case, this approach deserves a brief introduction before discussing the results.

In this model the scattering bodies are considered as polydisperse clusters constituted by monodisperse non-interacting spheres: i.e. aggregates formed by a variable number of identical rigid spheres. How this sub-units are packed is described by the fractal dimension (D_f): a three dimensional packing would result in a D_f equal to 3, while a D_f close to 2 would indicate a planar structure of the aggregate.

As the sub-unit of our system we choose a G-unit of lignin: in fact, it is known that in softwood pyrolysis oils more than 90% of pyrolytic lignines are constitute by G-units¹⁴. In order to assimilate the structure of the G-lignin to a sphere, we calculated the radius of gyration of an hypothetical ellipsoid (see figure 6):

$$R_g = \sqrt{\frac{1}{5}(a^2 + b^2 + c^2)} = \sqrt{\frac{1}{5}(4^2 + 2.6^2 + 0.7^2)} = 2.16 \text{ \AA} \quad (2)$$

where a , b and c are the semi-axes of the ellipsoid. This value was then used to calculate the radius of a sphere having the same radius of gyration:

$$R = \sqrt{\frac{5}{3}} R_g = 2.79 \text{ \AA} \quad (3)$$

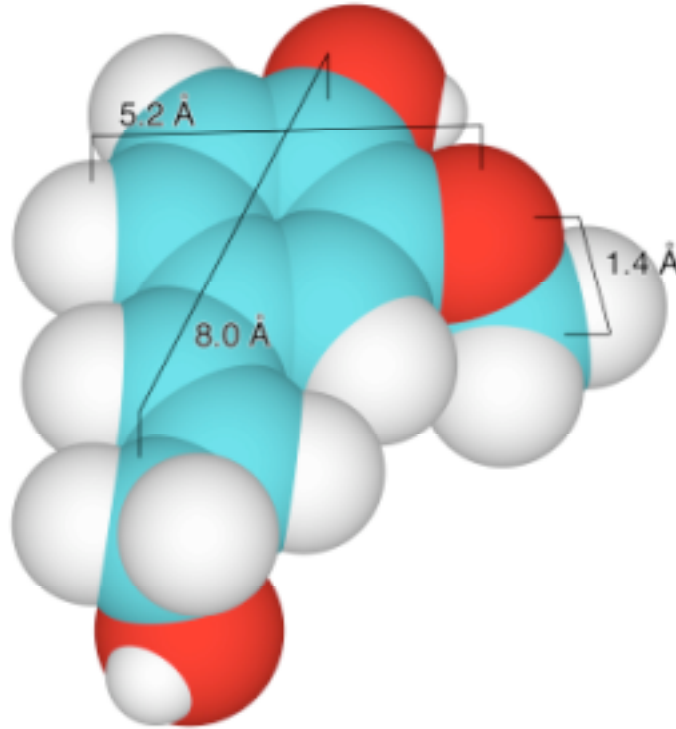


Figure 6. 3D visualization of the G unit of lignin. The values of the axes of the hypothetical ellipsoid used in the calculation of the radius of the sub-unit for the fractal model are shown.

The results of the fitting according to the fractal model are shown in figure 7. As reported in table 3, again the volume fraction of the scattering objects increases as a function of aging time, while the number of spherical sub-units per cluster (i.e. the aggregation number) increases during the first 4 months and is almost constant during the next 15 months.

Comparing the values of χ^2/n for the fractal model with both the cylindrical and the ellipsoidal models it is clear how the fractal structure is much more accurate in the description of the aggregates present in the BCO. In particular, the values are always lower than in the two previous cases and, moreover, the model is able to fit with the same accuracy fresh and old samples.

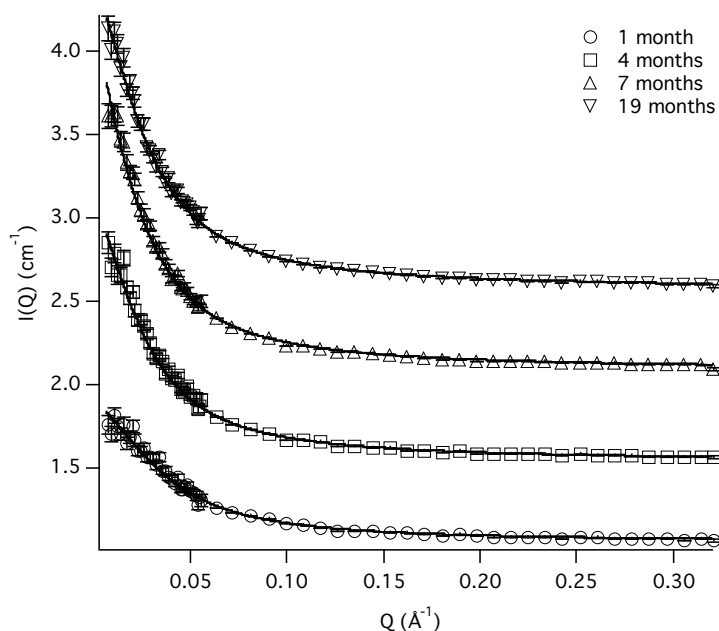


Figure 7. Fitting curves according to the fractal model (full lines) and experimental data (markers) of 1, 4, 7 and 19 months aged samples of BCO. 4, 7 and 19 months old sample data and fittings are offset respectively by a 0.5, 1 and 1.5 value.

With regards to the fractal dimension, its value is always between 1.4 and 1.5, i.e. the typical values of branched structures. If the pyrolytic lignins were formed by monomers, one would expect a well packed structure, like the globular lignin reported on the right in figure 8. Instead, the values obtained for the fractal dimension indicate a quite *open* structure, like the one shown on the left in figure 8. This structure was calculated by performing a geometry optimization of a molecule obtained combining three different tetramers formed by G lignin (three tetramers per type were combined). As shown in the figure, the

association of tetramers hardly takes to a well packed structure, in agreement with the results of our SANS investigation. This definitely confirms the thermal ejection theory¹⁶ and the hypothesis that aggregation of pyrolytic lignins is a fundamental process in the ageing of pyrolysis oils.

Table 3. Results obtained by fitting SANS experimental data according to the fractal model (see Appendix A).

Fractal Model Results				
Ageing Months	1	4	7	19
Volume Fraction	0.084	0.096	0.108	0.109
Aggregation Number	69.7	91.2	90.2	90.7
Fractal Dimension	1.49	1.41	1.41	1.42
χ^2/n	2.33	2.82	2.52	2.44

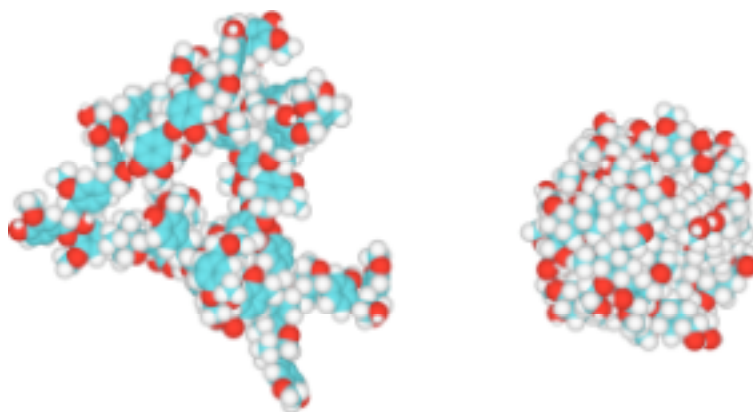


Figure 8. 3D structure of a globular lignin molecule (on the right) and an hypothetical pyrolytic lignin molecule characterized by the same molecular weight ($M_w \cong 6500 \text{ g mol}^{-1}$) and formed by the association of 9 G-lignin tetramers.

Conclusions

To be written

Appendix A. Models

Cylinders

The non-linear least-squares fitting of SANS data according to a polydisperse spherical form factor was performed by using the data analysis routines developed by the SANS group at the NIST Center for Neutron Research (Gaithersburg, USA). The routine was implemented in order to perform a self-consistent calculation of the contrast: i.e. the contrast is automatically calculated at each minimization cycle as a function of the volume fraction generated by the minimization routine. For more details, see appendix B.

The scattering intensity is calculated according to the following equations ¹⁹:

$$I(q) = \phi \cdot P(q) \quad (2)$$

$$P(q) = \frac{\phi}{V_{cyl}} \int_0^{\pi/2} f^2(q, \alpha) \sin \alpha d\alpha \quad (3)$$

$$f(q, \alpha) = 2(\rho_{cyl} - \rho_{solv})^2 V_{cyl} j_0\left(\frac{qL}{2} \cos \alpha\right) \frac{J_1(qr \sin \alpha)}{(qr \sin \alpha)} \quad (4)$$

$$j_0(x) = \sin(x)/x \quad (5)$$

where ϕ is the particle volume fraction, V_{cyl} is the volume of the cylinder, ρ_{cyl} and ρ_{solv} are, respectively, the scattering length densities of the cylinders and the solvent, r and L are the radius and the length of the cylinder, $J_1(x)$ is the first order Bessel function, and α is defined as the angle between the cylinder axis and the scattering vector, q . The integral over α in equation (3) averages the form factor over all the possible orientations of the cylinder with respect to q .

No interparticle interference effects (i.e. what is commonly called as *structure factor*) are included in this calculation. This means that we are not considering any interaction between cylinders. However, owing to the low volume fraction of the scattering objects, this assumption looks reasonable.

Ellipsoids

As in the cylinder case, the non-linear least-squares fitting of SANS data according to an ellipsoidal form factor was performed by using the data analysis routines developed by the SANS group at the NIST, implemented for the contrast calculation.

The scattering intensity is calculated according to the following equations²⁰:

$$I(q) = \phi \cdot P(q) \quad (6)$$

$$P(q) = \frac{\phi}{V_{ell}} (\rho_{ell} - \rho_{solv})^2 \int_0^1 f^2 [qr_b (1 + x^2(v^2 - 1))^{1/2}] dx + bkg \quad (7)$$

$$f(x) = 3V_{ell} \frac{(\sin x - x \cos x)}{x^3} \quad (8)$$

$$V_{ell} = \frac{4\pi}{3} r_a r_b^2 \quad (9)$$

$$v = \frac{r_a}{r_b} \quad (10)$$

where ϕ is the particle volume fraction, V_{ell} is the volume of the ellipsoid, ρ_{ell} and ρ_{solv} are, respectively, the scattering length densities of the cylinders and the solvent, and r_a and r_b are, respectively, the semi-axes along and perpendicular to the rotation axis of the ellipsoid.

As in the cylinder case, no interparticle interference effects are included in this calculation.

Fractals aggregates of non-interacting spheres:

In the approach by Chen and co-workers, it was assumed that the scattering bodies are constituted by polydisperse clusters, each cluster comprising k identical elementary sub-units. On this assumption, the scattering intensity of N_v clusters per unit volume is:

$$I(Q) = (\rho_{fract} - \rho_{solv})^2 A^2 \sum_{k=0}^{\infty} N(k) k^2 S_k(Q) \quad (11)$$

where $N(k)$ represents the number of clusters that contain k unit particles, ρ_{fract} ρ_{solv} are the neutron scattering length density of the particles constituting the fractal aggregate and of the solvent, respectively, and $S(k)$ is the intra-cluster structure factor. A proper $S_k(Q)$ has been given by Chen and Teixeira²¹ in the case of a fractal aggregate consisting of k elementary particles with a fractal dimension D_f :

$$S_k(Q) = \frac{\sin\left[(D_f - 1)\tan^{-1}(QR_k)\right]}{(D_f - 1)QR_k(1 + Q^2R_k^2)^{(D_f - 1)/2}} \quad (12)$$

where R_k is the radius of gyration of the k - cluster, related to the radius of gyration of the elementary particle R_p by the equation:

$$R_k = R_p k^{1/D_f} \quad (13)$$

Appendix B. Contrast Calculation

The PO system can be thought as lignin dispersion in an aqueous solution of organic molecules (that we have referred to as solvent in the previous section). Starting from this assumption the scattering length densities describing the interaction of neutrons with the two phases (lignin and solvent) can be calculated using the weight fraction of the scattering objects and the elemental analysis of the bio-oil and lignin through the following procedure.

The carbon, hydrogen and oxygen (CHO) content of the pine sawdust PO under investigation and its density are:

$$C_{pO}=45.3\%, H_{pO}=6.93\%, O_{pO}=47.77\%, d_{pO}=1.23 \text{ g/cm}^3$$

Yrjo and Anja, here we used an average of the values for three POs from pine you already published (Energy & Fuels, Vol. 17, No. 2, 2003 437). If you obtained different values for the PDU 15 02, just let us know them.

With regards to the CHO content of the lignin, it is known that in softwood G-units constitute more than 90% of pyrolytic lignins. Moreover, as reported previously in the case of an analogous PO produced by VTT¹⁵, most of the pyrolytic lignins have a molecular weight close to 800 g mol⁻¹. This corresponds to oligomers formed by four G-units. Therefore we used the CHO content of a hypothetical G-lignin tetramer: $C_{lign}=65.96\%$, $H_{lign}=5.96\%$, $O_{lign}=28.08\%$. With regards to the density, we used the typical value for lignin: $d_{lign}=1.46 \text{ g/cm}^3$.

The CHO content of the solvent can be calculated as:

$$C_{solv} = C_{BCO} - C_{lign} \frac{\phi_w}{(1 - \phi_w)} \quad (14)$$

$$H_{solv} = H_{BCO} - H_{lign} \frac{\phi_w}{(1 - \phi_w)} \quad (15)$$

$$O_{solv} = O_{BCO} - O_{lign} \frac{\phi_w}{(1 - \phi_w)} \quad (16)$$

where ϕ_w and ϕ_v are, respectively, the weight and volume fraction of lignin, and they are connected to the densities through the following equations:

$$\phi_w = \phi_v \frac{d_{lign}}{d_{BCO}} \quad (17)$$

$$d_{solv} = d_{BCO} \frac{(1 - \phi_w)}{(1 - \phi_v)} \quad (18)$$

The neutron scattering length density of lignin can be obtained as:

$$\rho_{lign} = \frac{(n_{C_{lign}} \cdot b_C + n_{H_{lign}} \cdot b_H + n_{O_{lign}} \cdot b_O) \cdot 10^{-15}}{\left[(n_{C_{lign}} \cdot PA_C + n_{H_{lign}} \cdot PA_H + n_{O_{lign}} \cdot PA_O) / d_{lign} \cdot 10^6 \right]} \cdot N_A \quad (19)$$

where:

$$n_{C_{lign}} = C_{lign} / PA_C; n_{H_{lign}} = H_{lign} / PA_H; n_{O_{lign}} = O_{lign} / PA_O \quad (20)$$

and

$$n_{C_{solv}} = C_{solv} / PA_C; n_{H_{solv}} = H_{solv} / PA_H; n_{O_{solv}} = O_{solv} / PA_O \quad (21)$$

PA_C , PA_H and PA_O are the atomic weight of C, H and O, respectively, b_C , b_H and b_O are their neutron scattering lengths and N_A is the Avogadro number.

In the same way the neutron scattering length density of solvent can be obtained as:

$$\rho_{solv} = \frac{(n_{C_{solv}} \cdot b_C + n_{H_{solv}} \cdot b_H + n_{O_{solv}} \cdot b_O) \cdot 10^{-15}}{\left[(n_{C_{solv}} \cdot PA_C + n_{H_{solv}} \cdot PA_H + n_{O_{solv}} \cdot PA_O) / d_{solv} \cdot 10^6 \right]} \cdot N_A \quad (22)$$

Finally, the contrast in cm^{-2} units is:

$$\Delta\rho = (\rho_{lign} - \rho_{solv}) \cdot 10^{-4} cm^{-2} \quad (23)$$

A new value for the volume fraction of scattering objects is generated during each minimization cycle of the non-linear least-squares fitting of SANS data. As a response to this value, the program automatically generates the new contrast value that is used for calculating the scattering intensity curve.

Acknowledgements

Authors thank Dr. J. Teixeira (LLB, CEA, Saclay) for help with the experimental setup and the Laboratoire Leon Brillouin (CEA, Saclay) for allocating neutron beam time at the PAXE (G5.4) spectrometer (Proposal Number 7034). Acknowledgments are also due to the European Union for support via the “HCM-Access to large scale facilities” Contract XXXXXXXX (LLB, Saclay, France). Finally, E.F., M.B. and P.B. acknowledge MIUR (PRIN-2003 grant) and the Consorzio Interuniversitario per lo Sviluppo dei Sistemi a Grande Interfase (CSGI, Florence, Italy) for partial financial support.

Dear Yrjo and Anja, since all these measurements were performed not using any resource coming from the European Project, we thought it would have been much simpler to keep this paper out from the project (that's why we haven't presented these results at last meeting). In this way we have not to ask permissions to the other partners to publish these data. Moreover all the expenses for traveling and staying at the Neutron Scattering Facility were not charged over the project, so this seems to us a reasonable decision. Just let us know if you agree with this arrangement.

If you have to acknowledge any person or grant for the oil production, just add a paragraph here.

REFERENCES

- (1) Yaman, S. *Energy Conv. Manag.* **2004**, *45*, 651-671.
- (2) Oasmaa, A.; Czernik, S. *Energy Fuels* **1999**, *13*, 914-921.
- (3) Leech, J.; Bridgwater, A. V.; Cuevas, A.; Maggi, R. In *Renewable Energy Development*; Zervos, A., Sala, M., Eds.: Venice (Italy), 1995, pp 340-345.
- (4) Sharma, R. K.; Bakhshi, N. N. *Energy Fuels* **1993**, *7*, 306-314.
- (5) Demirbas, A.; Demirbas, M. F. *Energ Source* **2003**, *25*, 317-329.
- (6) Herrera, P. S.; Creed, B. L.; Wong, C. M. *Abstr Pap Am Chem S* **1994**, *208*, 13-Fuel.
- (7) Chiamonti, D.; Bonini, A.; Fratini, E.; Tondi, G.; Gartner, K.; Bridgwater, A. V.; Grimm, H. P.; Soldaini, I.; Webster, A.; Baglioni, P. *Biomass Bioenerg.* **2003**, *25*, 85-99.
- (8) Baglioni, P.; Fratini, E.; Ricceri, R.; Sarti, G.; Chiamonti, D.; WO0102516, 1999.
- (9) Chiamonti, D.; Bonini, A.; Fratini, E.; Tondi, G.; Gartner, K.; Bridgwater, A. V.; Grimm, H. P.; Soldaini, I.; Webster, A.; Baglioni, P. *Biomass Bioenerg.* **2003**, *25*, 101-111.
- (10) Oasmaa, A.; Kuoppala, E. *Energy Fuels* **2003**, *17*, 1075-1084.
- (11) Diebold, J. P. In *Fast Pyrolysis of Biomass: A Handbook*; Bridgwater, A. T., Ed.; CPL Press: Newbury U.K., 2002; Vol. 2, pp 243-292.
- (12) Czernik, S.; Johnson, D. K.; Black, S. *Biomass and Bioenergy* **1994**, *7*, 187-192.
- (13) Sipila, K.; Kuoppala, E.; Fagernas, L.; Oasmaa, A. *Biomass Bioenerg.* **1998**, *14*, 103-113.
- (14) Scholze, B.; Meier, D. *J. Anal. Appl. Pyrolysis* **2001**, *60*, 41-54.
- (15) Scholze, B.; Hanser, C.; Meier, D. *J. Anal. Appl. Pyrolysis* **2001**, *58*, 387-400.
- (16) Piskorz, J.; Majerski, P.; Radlein, D. In *Biomass. A Growth Opportunity in Green Energy and Value-Added Products*; Overend, R. P., Chronet, E., Eds.; Elsevier: Amsterdam, 1999; Vol. 2, p 1153.
- (17) Liu, Y. C.; Sheu, E. Y.; Chen, S. H.; Storm, D. A. *Fuel* **1995**, *74*, 1352-1356.
- (18) Sheu, E. Y.; Liang, K. S.; Sinha, S. K.; Overfield, R. E. *Journal of Colloid and Interface Science* **1992**, *153*, 399-410.
- (19) Guinier, A.; Fournet, G. *Small Angle Scattering of X-Rays*; John Wiley: New York, 1955.
- (20) Feigin, L. A.; Svergun, D. I. *Structure Analysis by Small-Angle X-Ray and Neutron Scattering*; Plenum Press: New York, 1987.
- (21) Chen, S. H.; Teixeira, J. *Phys. Rev. Lett.* **1985**, *57*, 2583.